Ionospheric Total Electron Content and Electron Density Response Induced by the 8 April 2024 Total Solar Eclipse

Article *in* Advances in Space Research · December 2024

DOI: 10.1016/j.asr.2024.12.066

CITATIONS
0

READS
174

6 authors, including:

Xuan Le
Wuhan University
9 PUBLICATIONS **29** CITATIONS
SEE PROFILE

Dengkui Mei
Wuhan University
23 PUBLICATIONS **223** CITATIONS
SEE PROFILE

Ahmed Abdelaziz
Wuhan University
6 PUBLICATIONS **1** CITATION
SEE PROFILE

Xiaodong Ren
Wuhan University
74 PUBLICATIONS **2,216** CITATIONS
SEE PROFILE

Journal Pre-proofs

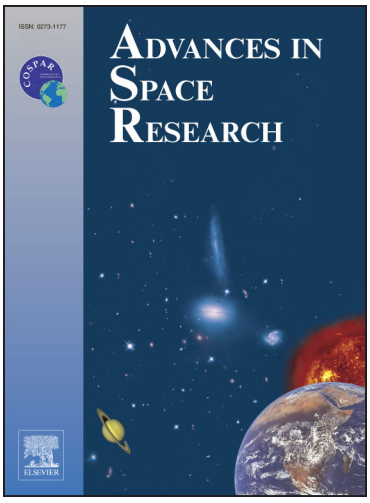

Ionospheric Total Electron Content and Electron Density Response Induced by the 8 April 2024 Total Solar Eclipse

Xuan Le, Dengkui Mei, Jinyuan Chen, Ahmed Abdelaziz, Xiaodong Ren, Xiaohong Zhang

PII: S0273-1177(24)01312-7
DOI: https://doi.org/10.1016/j.asr.2024.12.066
Reference: JASR 18055

To appear in: *Advances in Space Research*

Received Date: 17 September 2024
Revised Date: 22 December 2024
Accepted Date: 25 December 2024

Please cite this article as: Le, X., Mei, D., Chen, J., Abdelaziz, A., Ren, X., Zhang, X., Ionospheric Total Electron Content and Electron Density Response Induced by the 8 April 2024 Total Solar Eclipse, *Advances in Space Research* (2024), doi: https://doi.org/10.1016/j.asr.2024.12.066

Ionospheric Total Electron Content and Electron Density Response Induced by the 8 April 2024 Total Solar Eclipse

Xuan Le[1,2], Dengkui Mei[1,2], Jinyuan Chen[1,2], Ahmed Abdelaziz[4], Xiaodong Ren[1,2] and Xiaohong Zhang[1,2,3]

[1] School of Geodesy and Geomatics, Wuhan University, Wuhan 430079, Hubei, China

[2] Hubei Luojia Laboratory, Wuhan University, Wuhan 430079, Hubei, China

[3] Chinese Antarctic Center of Surveying and Mapping, Wuhan University, Wuhan 430079, Hubei, China

[4] State Key Laboratory of Information Engineering in Surveying, Mapping and Remote Sensing (LIESMARS), Wuhan University, Wuhan 430079, Hubei, China

Corresponding author: Xiaodong Ren (xdren@whu.edu.cn)

Abstract

Using data from nearly 2,000 ground-based GNSS observation stations, the response of two-dimensional total electron content (TEC) and three-dimensional electron density in the ionosphere during the solar eclipse on April 8, 2024 was investigated. The eclipse resulted in TEC decrease that lasted for over 7 hours, covering the entire United States. Approximately 60% of the obscuration region along the eclipse path experienced TEC depletes ranging from 20-40%. Following the eclipse, a widespread TEC enhancement was observed, propagating from high-latitude regions towards the equator. After the TEC enhancement, a secondary large-scale TEC depletion phenomenon was observed for the first time, with the depletion belt mainly concentrated near the eclipse path. The TEC enhancement and TEC secondary depletion exhibit distinct variations in latitude and longitude, respectively. The overall three-dimensional electron density in the ionosphere displayed consistent behavior with TEC, but exhibits significant altitude-dependent characteristics. The maximum electron density decrease occurred near the F2 peak at an altitude of 300 km, with a magnitude of up to 30%. Ionospheric plasma disturbances triggered by the eclipse may be associated with dynamic processes related to plasma flux from the upper ionosphere.

Keywords

Total solar eclipse, Ionosphere, Total electron content (TEC), Ionospheric electron density, Global Navigation Satellite System (GNSS)

1 Introduction

The solar eclipse is a celestial phenomenon where the Moon moves between the Sun and the Earth, completely or partially blocking the sunlight (Huang et al., 2020). The Moon not only obstructs visible light but also blocks the solar extreme ultraviolet (EUV) flux. This provides an excellent natural experiment for exploring the transient effects of solar radiation on the ionosphere system (Aa et al., 2020). Over past decades, studies have investigated the ionospheric response to solar eclipses using various ground-based and space-based observational techniques, such as sparsely distributed ionosondes (Reinisch et al., 2018; Chen et al., 2013; Evans et al., 1965), high-frequency Doppler measurements (Chen et al., 2010; Mishin et al., 2012; Moses et al., 2021), and incoherent scatter radars (Baron et al., 1973; Bullett et al., 2018; Panasenko et al., 2019). In the late twentieth century, research began to study the ionospheric response during solar eclipses using GPS data (Afraimovich et al., 1998; Tsai et al., 1999; Boitman et al., 1999; Baran et al., 2003). Ground-based observations from the Global Navigation Satellite System (GNSS) and in-situ measurements from low Earth orbit satellites (LEO) have been widely utilized (Tsai & Liu, 1999; Ding et al, 2010; Pradipta et al., 2018; Cherniak & Zakharenkova, 2018; Perry et al., 2019; Zhang et al., 2020; Hussien et al., 2020; Kundu et al., 2022). Additionally, the response of the ionosphere-thermosphere to solar eclipses has been extensively studied through numerical simulations techniques (Müller-Wodarg et al, 1998; Wu et al, 2018; Dang et al., 2018; Lei et al., 2018; Le et al., 2020).

During a total solar eclipse, the supersonic motion of the Moon's shadow leads to a significant reduction in solar EUV flux, causing rapid cooling of the passing ionospheric region (Zhang et al., 2017). The direct ionospheric response to a solar eclipse includes depletion of

electron density and Total Electron Content (TEC), varying at different ionospheric altitudes and latitudes (Aa et al., 2021). Electron density reductions during a solar eclipse can reach 30-50%, with the maximum decrease typically occurring near the F2 layer peak height (hmF2) (Aa et al., 2024a). Solar eclipses impact the ionosphere through multiple processes, such as photochemical reactions, neutral composition transport, and plasma temperature variations (Bullett et al., 2018; Cherniak & Zakharenkova, 2018; Huang et al., 2020). Different ionospheric regions are influenced by these processes to varying degrees. For example, while the F2 layer response during an eclipse is affected by various processes, it is primarily dominated by transport (Bullett et al., 2018). Meanwhile, the F1 layer's response is mainly governed by photochemical reactions (Müller-Wodarg et al, 1998). Additionally, TEC depletes during a total solar eclipse can reach 30-40% in mid-latitude regions and a decrease of 10-30% at high latitudes. The ionosphere at equatorial latitudes, which is associated with total solar eclipses, exhibits exceptionally complex behavior due to the fountain effect, with TEC dissipations exceeding 40% (Cherniak & Zakharenkova, 2018).

Additionally, the ionosphere can observe sustained electron density enhancement effects related to solar eclipses. Such phenomena typically occur at the beginning of an eclipse (Evans et al., 1965; Cheng et al., 1992; Vyas et al., 2012). For example, Evans (1965) observed an enhancement in foF2 during the initial phase of the eclipse using six ionosondes distributed across Alaska, Canada, and North America, which is largely attributed to the downward migration of plasma (Boitman et al., 1999). Some studies have also observed electron density enhancement effects after the eclipse (Huang et al., 1999; Chen et al., 2013; Chermiak & Zakharenkova, 2018; Wu et al., 2018). Chen et al. (2013) recorded foF2 enhancements in the ionosphere after the eclipse ended using an ionosonde network during the 15 January, 2010 eclipse. Subsequently, Chermiak and Zakharenkova (2018) observed a 20-30% increase in TEC over North America after the eclipse using reconstructed TEC data from GPS and GLONASS observations. The Swarm and DMSP satellites also detected electron density enhancements at an ionospheric altitude of 450 km.

The occurrence of a total solar eclipse lasting for an extended period of time in a densely instrumented network is an extremely rare event. On 21 August 2017, the first total solar eclipse to traverse thousands of dense GNSS observation networks in the United States has been reported in detail (Huba et al., 2017; Bullett et al., 2018; Zhang et al., 2021; Lin et al., 2018; Coster et al., 2017; Wu et al., 2018). Utilizing high-precision, high spatial resolution, and all-weather continuous monitoring provided by GNSS techniques, the two-dimensional/three-dimensional (2-D/3-D) ionospheric responses associated with this event were extensively investigated. For instance, large-scale TEC depletions exceeding 40% and 3-D electron density reductions were observed (Reinisch et al., 2018; Coster et al., 2017; Chen et al., 2022), as well as post-eclipse persistent ionospheric effects (Wu et al., 2018; Lei et al., 2018), and the evolution and development of traveling ionospheric disturbance and ionospheric bow waves (Zhang et al., 2017; Cherniak & Zakharenkova, 2018; Coster et al., 2017; Pradipta et al., 2018; Perry et al., 2019).

On 8 April 2024, a total solar eclipse traverse from low-latitude regions to North America, crossing through Mexico, the United States, and southeastern Canada in a northeast direction. The path of the eclipse penumbra once again covers the contiguous United States with a densely populated GNSS observation network, providing millions of lines of sight through the ionospheric layer. In addition, the total solar eclipse occurs during the peak of solar activity, with the umbra

crossing through low and middle latitude regions. This provides a completely new perspective that is different from the dramatic ionospheric changes of the 2017 total solar eclipse.

Recently, Aa et al. (2024b) reported the initial enhancement and eclipse-induced ionospheric depletion during the solar eclipse on 8 April 2024 through multi-instrument observations and data assimilation techniques, but the post-eclipse ionospheric enhancement phenomenon has not been studied yet. In this paper, we comprehensively investigate the ionospheric response during and the secondary response after the solar eclipse utilizing a GNSS network through 2-D ionospheric TEC extraction and 3-D ionospheric tomography.

2 Solar, Interplanetary and Geomagnetic Conditions Analysis

Figure 1 illustrates the variations of F10.7, Interplanetary Magnetic Field (IMF) Bz, SYM-H, and Kp indices component from 3-13 April 2024. It can be clearly seen that there is a significant difference in F10.7 during the period, with the value increasing from 111.7 to 161.9 SFU. During the same period, the IMF Bz component fluctuates around 0, indicating that the IMF does not show a clear direction. The SYM-H index shows a significant enhancement on 4 April during a slight northward IMF, suggesting a slight increase in ring current intensity on that day. Additionally, the SYM-H index slightly decreases on April 6, with a minimum value close to -40nT. The maximum value of the Kp index remains below 3.4, indicating low geomagnetic activity throughout the period of 3-13 April.

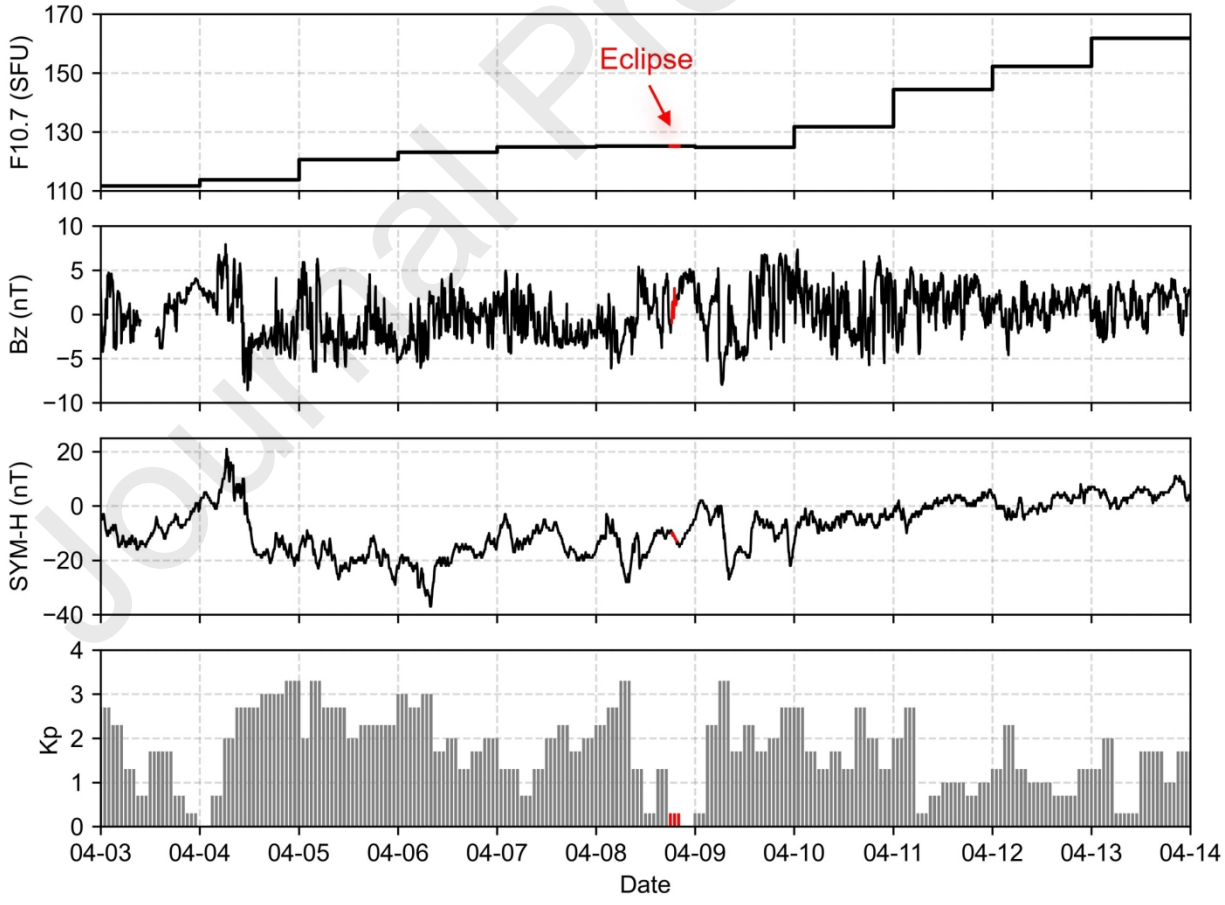

Fig 1 Time series of solar, interplanetary, and geomagnetic parameters (i.e., F10.7, IMF Bz , SMY-H and Kp indices).

3 Observation and method

The 2-D TEC data for the contiguous United States is obtained from the Madrigal Database developed by the Haystack Observatory at the Massachusetts Institute of Technology (Vierinen et al., 2016). The TEC data in this database is released in a gridded format and is derived from a dense global network of over 6,000 GNSS receivers. These TEC values are averaged and distributed into a grid with a resolution of 1° × 1° in latitude and longitude and are generated every 5 minutes (Aa et al., 2024a). To study the ionospheric response during a solar eclipse, the differential TEC (DTEC) values for the eclipse period are obtained by subtracting the background TEC values. The background TEC is typically obtained by averaging TEC values during a period of low solar activity and geomagnetically quiet, before and after the eclipse (Cherniak & Zakharenkova et al., 2018). Taking into account the solar activity and geomagnetic conditions, we have selected the TEC data from the day before the eclipse (April 7) and the day after the eclipse (April 9) as the source of reference in this study.

As the Madrigal database currently does not provide slant TEC (STEC) data during the solar eclipse, the results of 3-D ionospheric tomography are obtained using a dense GNSS network consisting of approximately 1600 Continuously Operating Reference Stations (CORS) in North America. Figure 2a shows the distribution of these GNSS stations, which provide millions of sTEC along the line-of-sight between satellites and receivers during the solar eclipse due to their dense coverage. The sTEC values are extracted from the raw observations using the carrier-to-code leveling method (Ciraolo et al., 2007). A cutoff elevation angle of 30° is chosen to mitigate multipath effect error (Ren et al., 2024). Using the compressed sensing technique (CST) for ionospheric tomography, a rapid construction of ionospheric electron density maps for the continental United States during the solar eclipse is achieved. The detailed process can be found in our previous study (Mei et al., 2023). This method reconstructs a high-precision, high-temporal-resolution 3-D ionospheric model using observations from a relatively short period of time. The tomographic model has a spatial resolution of 1° × 1° in latitude and longitude, and covers a height range of 100 to 1000 km. Within the height range of 100 to 600 km, the vertical spacing is 50 km, while within the range of 600 to 1000 km, the spacing is 100 km.

4 Results

The total solar eclipse on 8 April 2024, began at 16:42 UT and ended at 19:54 UT. The umbral shadow of the eclipse crossed the continental United States from the southern region in a northeast direction, lasting approximately 78 minutes from 18:16 UT to 19:34 UT. Figure 2a displays the GNSS station locations in the continental United States, along with the eclipse path and contour lines indicating the extent of obscuration. The dense GNSS network enables tracking of the ionospheric effects during the eclipse under varying levels of obscuration, ranging from 25 to 100%. To observe the ionospheric behavior, we have selected four stations from the network shown in Figure 2a with different latitudes. As depicted in Figure 2b, these stations are located within or in close proximity to the umbral path of the eclipse.

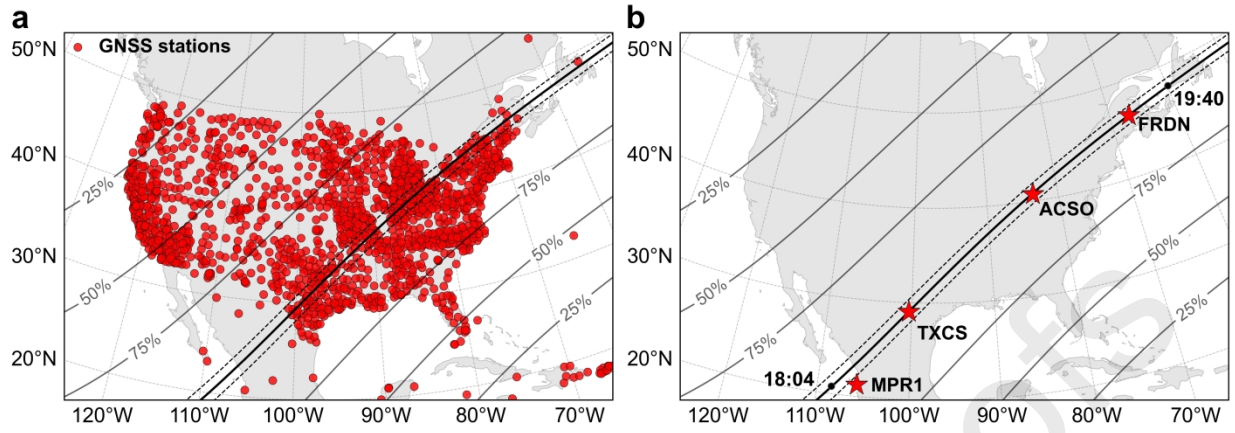

Fig 2 (a) The geographical locations of CORS stations in the continental United States overlaid with the path of the umbral shadow during the total eclipse (black line) and contour lines representing 75%, 50%, and 25% of the penumbra (gray lines). (b) The location of four GNSS stations that are either within or close to the eclipse path (red pentagrams).

Figure 3 presents the variation of vertical TEC (VTEC) observed from GPS satellites during the solar eclipse period compared to the reference day. The TEC values for the reference day are calculated as the average values for one day before (7 April) and after (9 April) the eclipse. TEC is measured in TECU, where 1 TECU is equal to 10^{16} el/m^2. During the eclipse, the ionospheric TEC exhibits significant deviations from normal climatic behavior. The TEC curves for all stations gradually decrease after the initial contact with the penumbra. The maximum decrease in TEC usually occurs approximately 20-40 minutes after the passage of the umbral shadow. Subsequently, the TEC curves gradually increase but remain lower than the reference values. Additionally, the eclipse's impact on the ionosphere shows latitude variations, where the two stations located above 40° latitude experience a higher decrease in TEC during the eclipse compared to the other two stations. Notably, an enhancement in ionospheric electron density was observed at the ACSO station, located at approximately 40°N latitude, prior to the eclipse. This phenomenon was also reported by Aa et al (2024), and we will provide further explanation in the discussion.

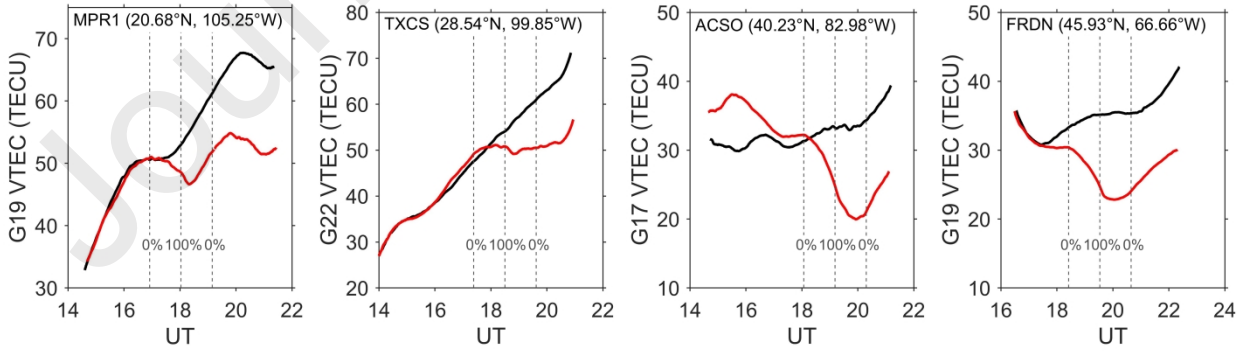

Fig 3 The variation of GPS VTEC with respect to time (UT) during the eclipse period (red curve) and the reference day (black curve); vertical dashed lines depict the start, maximum, and end times of the eclipse.

To comprehensively study the high spatiotemporal resolution variations in the ionosphere caused by solar eclipses, we performed differentials on the TEC data from the Madrigal database. It can be observed from Figure 3 that the ionosphere on the day of the eclipse (8 April) did not fully recover to the reference level. Therefore, the TEC data from the day after the eclipse (9 April) were also differentially processed. Since there was a significant difference in F10.7 between 9 April and 10 April (from Figure 1), the reference TEC was calculated by averaging the values from the period unaffected by the eclipse on April 7 and April 8.The high-resolution dTEC maps were constructed with a grid size of 1° × 1° and were generated every 5 minutes starting from 2:30 UT. Figures 4a and 4b reveals the dTEC values and percentage dTEC values at specific moments. A complete set of dTEC and percentage dTEC maps from 15:00 UT on April 8th to 15:00 UT on April 9th in 2024 can be found in Movie S1 (supporting information).

At 16:02:30 UT on 8 April 2024, prior to the solar eclipse, we observed slight variations within ±3 TECU in most parts of the continental United States. However, in the eastern region, the dTEC was 5-10 TECU higher than the reference value (enhancement effect), consistent with the observations from ACSO station (Figure 3). At 18:12:30 UT, the total eclipse approached the southwest United States, with the penumbral shadow covering over half of the U.S. The ionospheric enhancement effect in the eastern region started to diminish, and a reduction of approximately 5 TECU (~15%) in TEC values occurred within 75% of the shadowed region. As the eclipse reached the central United States at 18:52:30 UT, the penumbral shadow covered the majority of the continental United States, and the enhancement effect in the eastern ionosphere disappeared, giving way to dominant ionospheric depletion. The eclipse left the northeastern United States at 19:42:30 UT, and during the period passing over the United States, the ionosphere further underwent evolution. The dissipation of TEC was primarily concentrated within the 50% penumbral shadow region of the eclipse, resulting in a reduction of approximately 8-12 TECU (~20-40%). From Figure 4 and Movie S1 (16:02:30-19:42:30 UTC), it can be observed that: (1) the zone with the most drastic TEC changes expanded from 80% solar obscuration region at the beginning to 60% region; (2) TEC depletion in the northwest United States during the eclipse was minimal (within ±3 TECU), much weaker than in the eastern region; and (3) in the eastern area with the enhancement effect, the ionospheric response to the eclipse exhibited a delay of approximately 30 minutes compared to other areas.

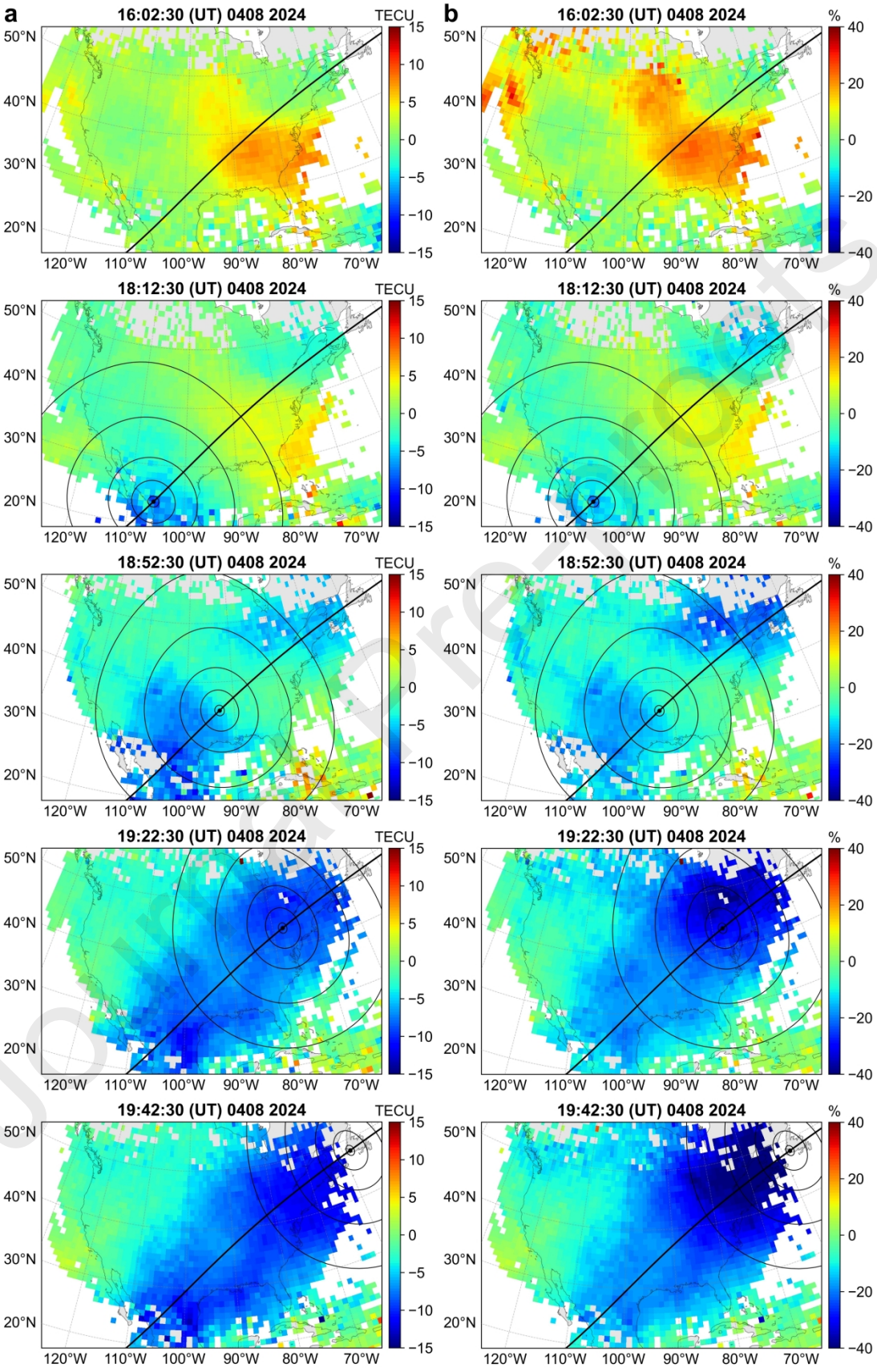

Fig 4 2D maps of (a) dTEC values and (b) percentage dTEC values at specific moments during the solar eclipse on 8 April 2024. The thick black line represents the path of the solar eclipse, while the thin lines depict approximately 100%, 90%, 75%, 50%, and 25% solar obscuration zones. A complete set of two-dimensional maps at 5-minute intervals is provided in Movie S1.

Figure 5 shows that the impact of the solar eclipse on the ionosphere lasted for nearly 7 hours. Following the end of the eclipse, the ionospheric TEC did not immediately enter the recovery phase but continued to deplete and spread across the entire continental United States (23:02:30 UT). TEC depletion reached 5-10 TECU (approximately 20%) in the northwest region. Subsequently, the TEC in all regions began to recover and reached the pre-eclipse level at 1:52:30 UT. It is worth noting that at this time, there was an enhancement of ionospheric TEC in high-latitude areas (Figure 5b) and continued to increase. The pronounced TEC enhancement occurred at 3:42:30 UT when a large TEC enhancement belt reached the southern United States, covering the majority of the continental United States, with a TEC increase of approximately 3-7 TECU (around 20-40%). Movie S1 provides a more detailed presentation of the TEC enhancement evolution. The TEC enhancement phenomenon initially appeared in high-latitude regions and gradually spread towards the equatorial direction. It covered the entire mainland United States at 4:32:30 UT and then gradually moved westward. According to the report by Cherniak et al. (2017), this phenomenon is likely related to the downward plasma flux in the plasma layer caused by the decrease in plasma temperature during the eclipse.

After the TEC enhancement came to an end, the ionosphere experienced widespread TEC depletion once again. According to Figure 5 and Movie S1, this TEC depletion initially originated from the southeastern coast of the United States and subsequently spread to the entire east coast. Around 9:22:30 UT, the secondary depletion of TEC reached its peak, with a maximum decrease of -7 TECU (approximately 40%). The TEC depletion belt then moved southward and persisted until around 12:37 UT when it disappeared.

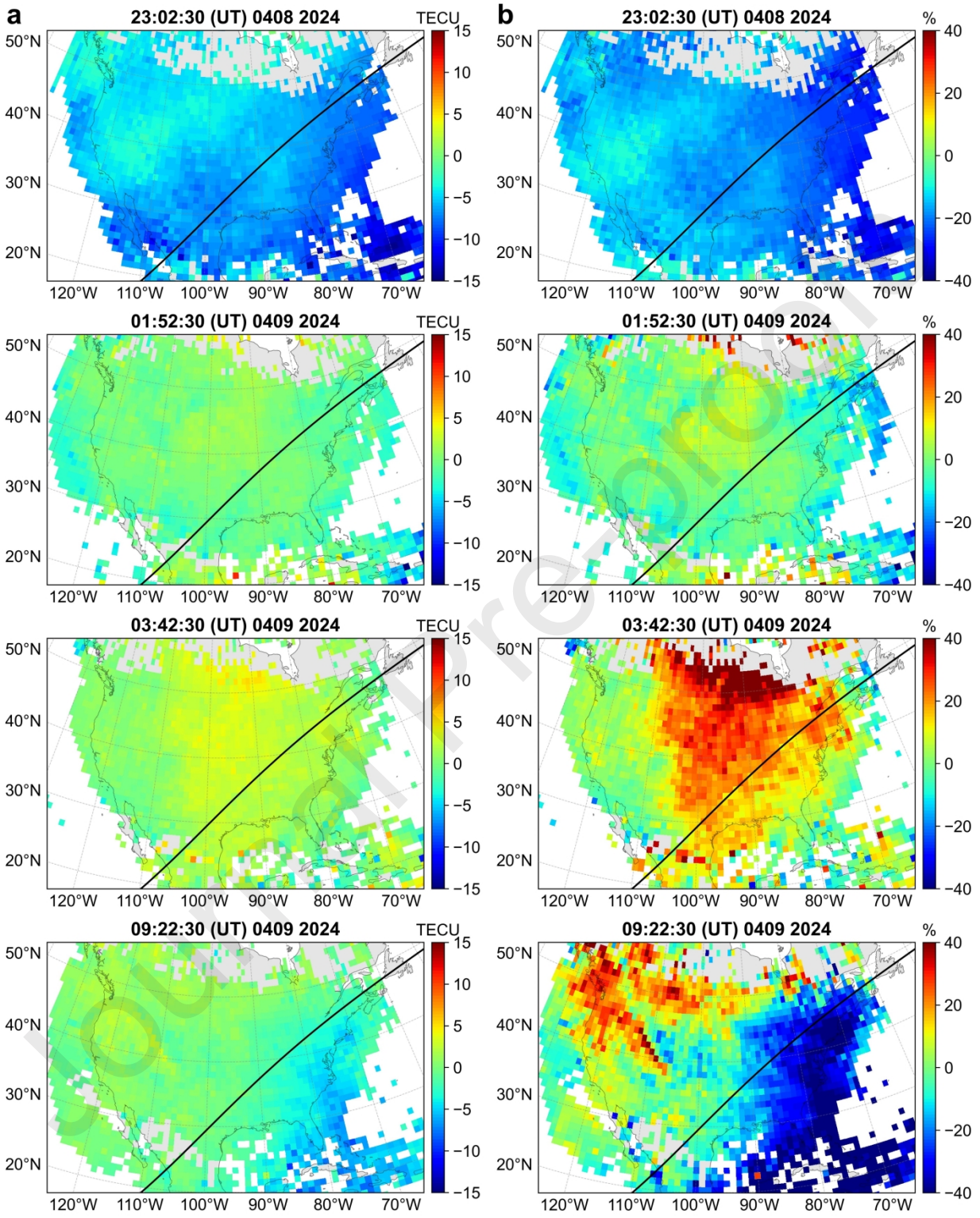

Fig 5 2D maps of (a) dTEC values and (b) percentage dTEC values at specific moments after the solar eclipse on 8-9 April 2024. A complete set of two-dimensional maps at 5-minute intervals is provided in Movie S1.

To analyze the horizontal and vertical effects, we compared the evolution of dTEC variation with time caused by the solar eclipse. Figures 6a and 6b show temporal variations in the percentage of the dTEC value along latitudes (from top to bottom, 50°N-20°N) and longitudes (from top to bottom, 110°W-80°W), respectively. After the occurrence of the solar eclipse, the ionospheric TEC experienced a significant decrease followed by a sustained enhancement. After the occurrence of the solar eclipse, the ionospheric TEC experienced a significant decrease followed by a sustained enhancement, which is an interesting point to focus on in this study.

The TEC response caused by the solar eclipse persisted from around 18:00 UT until around 14:00 UT the next day, and there were significant differences observed at different latitudes and longitudes. The initial TEC depletion phenomenon had the widest coverage and was observable at all latitudes and longitudes. The TEC depletion band primarily appeared in the northeastern United States (dTEC at 50°N and 80°W), reaching a maximum of approximately 40%. The maximum magnitude of TEC depletion slightly decreased with decreasing latitude. As longitude increased (moving westward), the magnitude of TEC depletion weakened more significantly. The TEC enhancement phenomenon occurred approximately 8 hours after the solar eclipse (around 2:00 UT on 9 April) and nearly covered the entire contiguous United States. The TEC enhancement band initially appeared in the high latitude region (50°N-60°N) with longitudes ranging from 80°W to 100°W. The TEC enhancement band gradually spread to lower latitude regions over time while also moving westward. As latitude decreased, the propagation range and magnitude of TEC enhancement decreased as well, with the enhancement magnitude decreasing from approximately 40% (at 50°N) to 20% (at 30°N). The propagation range of the TEC enhancement phenomenon also exhibited longitude dependence, being smaller in the eastern region of the United States compared to the western region. The second persistent TEC depletion phenomenon occurred at around 8:00 UT on the day following the solar eclipse and primarily occurred in the eastern United States (20°N-45°N, 80°W-100°W). In contrast to the TEC enhancement phenomenon, the second persistent TEC depletion did not originate from high-latitude regions but rather originated from the southeastern part of the United States and rapidly spread northwestward. Combining Figure 6 and Movie S1, it can be observed that the TEC depletion band was predominantly concentrated near the solar eclipse path and did not propagate to the northwestern part of the United States. Around 9:45 UT, the TEC depletion band reached its maximum extent, covering the entire southeastern United States, and subsequently gradually propagated to the south before disappearing around 12:30 UT.

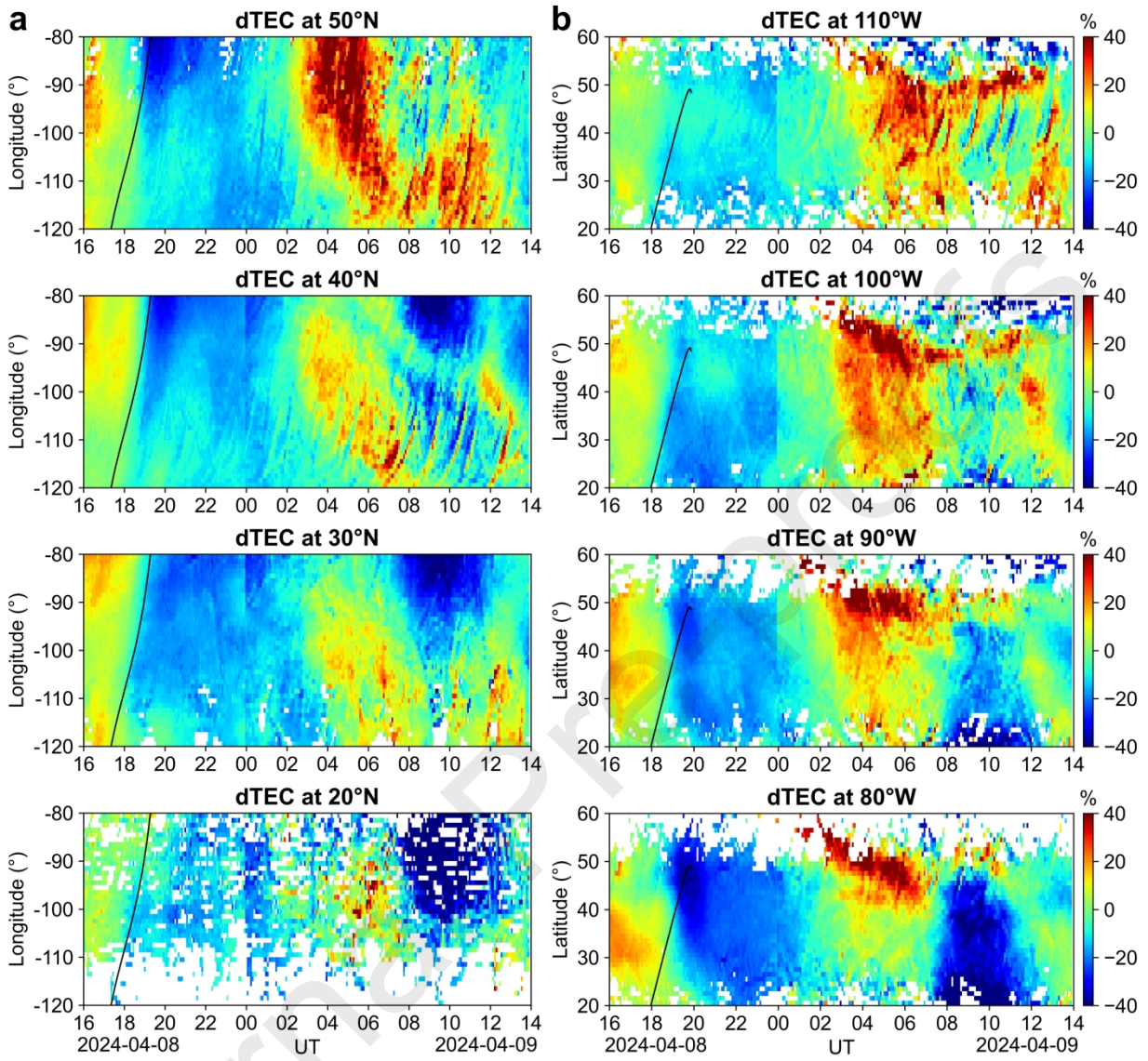

Fig 6 (a) The variation of the percentage of dTEC values with longitude and time for different latitudes (20°N-50°N) in the contiguous United States; the curves represent the longitudinal variation of the solar eclipse's umbra with time. (b) The variation of the percentage of dTEC values with longitude and time for different longitudes (80°W-110°W) in the contiguous United States; the curves represent the latitudinal variation of the solar eclipse's umbra with time.

To provide a more comprehensive understanding of the high spatiotemporal variation response of the ionosphere during the solar eclipse, we constructed a 3D electron density model during the eclipse period. The high-resolution electron density maps were created using a grid with a resolution of 1° × 1° in latitude and longitude, and a height of 50 km. The same differencing method used for generating the 2D TEC maps was applied to obtain differential Ne (dNe) maps for each layer, with a new map generated every 30 minutes starting from 17:30:00 UT. Since the 2D dTEC maps already effectively display the latitudinal and longitudinal variations of the

ionosphere, the focus of the 3D results is on the response of electron density at different altitudes during the solar eclipse.

Figure 7 illustrates the horizontal distribution of dNe values and the percentage of dNe values within the 50% contour of the penumbral shadow (the eastern United States) at specific moments during the solar eclipse. At 17:30:00 UT, just before the eclipse, the electron density was slightly higher than the reference day (ionospheric enhancement), with a maximum dNe value of 4×10^{11} el/m^3 (~20%). As the 25% contour of the penumbral shadow arrived, the ionospheric enhancement gradually weakened and almost disappeared by 18:30:00 UT. At 19:00:00 UT, when the eclipse began to reach the region, significant depletions were observed in the areas that had been crossed, with dNe reaching -2×10^{11} el/m^3 (~ -12%). As the eclipse progressed, noticeable reductions in dNe were observed at all altitudes, with the most severe TEC depletion occurring in the southeastern part of the eclipse path at 20:00 UT, where dNe even reached -5×10^{11} el/m^3 (~ -30%). Subsequently, the TEC depletion gradually weakened.

A complete set of dNe and percentage dNe maps from 17:00 UT on 8 April to 13:30 UT on 9 April 2024 can be found in Movie S2 (supporting information). From Movie S2, the subsequent enhancement and secondary depletion of the ionospheric Ne are consistent with the behavior of ionospheric TEC. It can be observed from Figure 7b that the Ne enhancement reaches its peak around 4:00:00 UT, with a dNe of approximately 2×10^{11} el/m^3 (~30%); the secondary Ne depletion reaches its peak around 9:30:00 UT, with a dNe of approximately 2×10^{11} el/m^3 (~30%). Additionally, throughout the entire eclipse process, there is consistency in dNe at all ionospheric heights, with the observation of two TEC depletions and the TEC enhancement after the eclipse. However, there are significant differences in the percentage of Ne depletion and enhancement at different ionospheric heights, with the maximum variation (~30%) observed at around 300 kilometers, possibly near the peak of the F2 layer. Below 250 kilometers or above 450 kilometers, the range of variations is only between -10% and 10%.

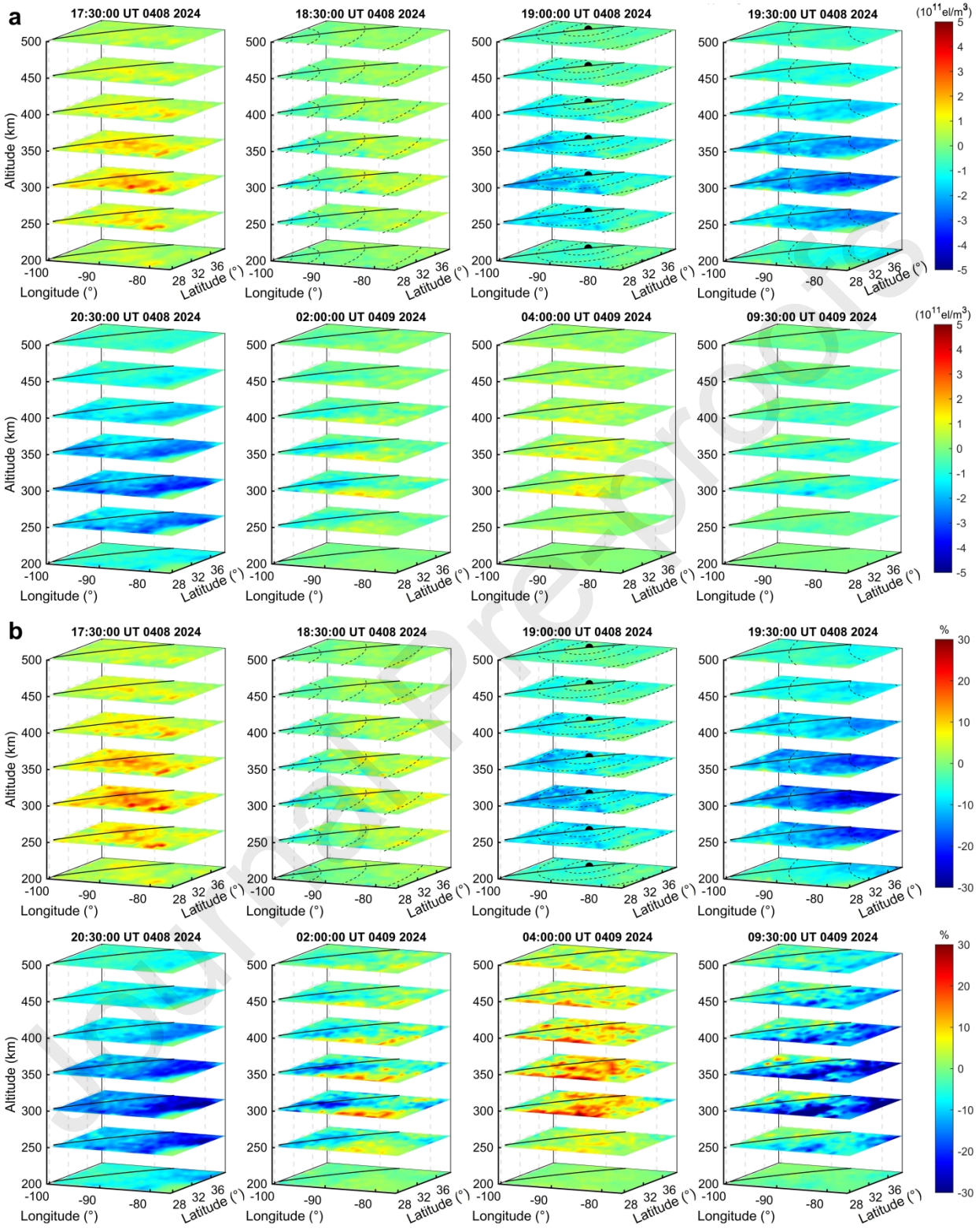

Fig 7 3D maps of (a) dNe values and (b) percentage dNe values at specific moments during 8-9 April 2024. The thick black line represents the path of the solar eclipse, while the dotted lines

depict approximately 75%, 50%, and 25% solar obscuration zones. A complete set of three-dimensional maps at 30-minute intervals is provided in Movie S2.

5 Discussion

In the subsequent sections, we will systematically review the characteristics of our observational results, compare them with previous works, and discuss possible reasons for the ionospheric enhancement phenomenon after the solar eclipse.

During the passage of the solar eclipse, there was a significant decrease in ionospheric TEC in approximately 60% of the obscuration region along the eclipse path, with a depletion magnitude of around 8-12 TECU (~20-40%). Following the passage of the eclipse's umbral shadow, the TEC depletion was delayed by 20-40 minutes, with the maximum delay occurring in the region around latitude 40°. This delay can be attributed to the pre-eclipse ionospheric enhancement effect in the area. The TEC depletion spread across the entire continental United States after the eclipse and took approximately 7 hours to recover fully. The previous studies on ionospheric response to solar eclipses through GNSS TEC observations mainly focused on the 2017 total solar eclipse event in the United States. The TEC decrease caused by the 2017 eclipse showed a delay of 8-20 minutes after the maximum eclipse, with an average reduction of approximately 4-6 TEC units (~30-40%), and returned to reference values within about 1 hour (Cherniak & Zakharenkova, 2018; Coster et al., 2017). The differences between these two events are mainly attributed to solar activity, with the ionospheric background value being higher during high solar activity year (2024), leading to a much larger total TEC decrease and longer recovery time compared to low solar activity year (2017).

The TEC enhancement after the eclipse was also one of the most significant features in this particular event. Due to the spreading effect of the ionospheric TEC depletion, the TEC enhancement in this event occurred approximately 7 hours after the eclipse, which is 5 hours later compared to the TEC enhancement observed after the 2017 eclipse (Cherniak & Zakharenkova et al., 2018). The TEC enhancement first appeared in high-latitude regions and gradually spread towards the equatorial direction, covering the entire continental United States before gradually moving westward. Additionally, there were latitude differences in the TEC enhancement phenomenon. As latitude decreased, the propagation range and magnitude of the TEC enhancement gradually diminished. A secondary widespread TEC depletion occurred after the TEC enhancement. This TEC depletion originated from the southeastern coast of the United States and subsequently spread throughout the southeastern region. The TEC depletion belt was primarily concentrated near the eclipse path and exhibited clear longitude dependence.

The results of the three-dimensional electron density in the ionosphere are consistent with the response of TEC, as both observed the two TEC depletions and the TEC enhancement after the eclipse. Additionally, the dNe at different altitudes in the ionosphere to the eclipse exhibits a strong dependence on altitude. There are significant differences in the percentage of dNe depletion and enhancement at different ionospheric heights, with the largest variations (~30%) observed at around 300 kilometers, possibly near the peak of the F2 layer.

The TEC enhancement phenomenon after a solar eclipse has been notably reported and analyzed in previous studies, reflecting the complex interactions in ionospheric dynamics after an

eclipse. Chen et al. (2013) observed nighttime enhancements in electron density after the solar eclipse on 15 January 2010. They suggested that the enhancement resulted from a downward plasma flux from the top ionosphere, likely stimulated by the decrease in plasma temperature during the eclipse. Similar views were also expressed by Cherniak et al. (2017) in their report on TEC enhancement after the 2017 eclipse. Furthermore, Wu et al. (2018) emphasized that the transportation process of neutral components also plays a significant role in driving the post-eclipse TEC enhancement, based on results generated by the Global Ionosphere-Thermosphere Model (GITM). Their findings indicated that the divergence of horizontal winds significantly increased the number density of Oxygen (O) at a height of 300 km. At the same altitude, the molecular number density of Nitrogen (N_2) did not show a significant increase, resulting in a rise in the O/N_2 ratio. This is likely the reason for the significant increase in plasma density in the F layer after the eclipse. In the ionospheric tomography results shown in Figure 5, we can see that the most pronounced post-eclipse rise in the ionosphere occurs around a height of 300 km, consistent with the predictions made by Wu et al. (2018). Therefore, the ionospheric plasma disturbances after a solar eclipse can be superimposed with dynamic processes associated with plasma flux from the upper ionosphere, representing secondary responses after the eclipse. The secondary TEC depletion phenomena also originate from these dynamic processes, potentially due to a decrease in the O/N_2 ratio. Further confirmation is required through simulation work by a coupled thermosphere/ionosphere/plasma layer dynamic system in the future.

6 Summary

On 8 April 2024, a total solar eclipse once again covered a significant portion of the continental United States, with a dense GNSS observation network comprising millions of line-of-sight paths through the ionosphere. It occurred during a period of solar maximum activity, providing a fresh perspective that differs entirely from the intense ionospheric variations observed during the low solar activity eclipse in 2017. By utilizing observations from nearly 2,000 GNSS stations, a detailed investigation of the response of ionospheric TEC and three-dimensional electron density to this total solar eclipse was conducted for the first time. The main results are summarized as follows:

1. A significant decrease in ionospheric TEC of about 20-40% was observed during the solar eclipse. The TEC decrease showed a delay of 20-40 minutes after the passage of the eclipse, with the maximum delay observed around 40° latitude, primarily due to the ionospheric enhancement effect before the eclipse in that region. The ionospheric TEC depletion extended across the entire continental US after the eclipse, taking nearly 7 hours to fully recover.

2. A notable TEC enhancement was observed after the eclipse, likely due to the spread of the ionospheric TEC depletion effect. Additionally, there were latitude differences in the TEC enhancement phenomenon, with the propagation range and enhancement amplitude gradually decreasing as latitude decreased.

3. Following the disappearance of the TEC enhancement phenomenon, a secondary widespread TEC depletion was observed in the ionosphere. The TEC depletion zones were mainly concentrated near the path of the eclipse, showing clear longitude dependence.

4. The results of ionospheric three-dimensional electron density were consistent with the TEC response. The response of dNe at different altitudes in the ionosphere to the eclipse was highly altitude-dependent. The largest changes (30%) were observed at 300 km altitude, while at altitudes below 250 km or above 450 km, the range of variation was only between -10% and 10%.

Acknowledgments

We acknowledge use of F10.7 data from National Aeronautics and Space Administration (NASA, via https://omniweb.gsfc.nasa.gov/form/dx1.html); GNSS MGEX RINEX data from CORS (https://geodesy.noaa.gov/CORS/data.shtml), IGS (https://cddis.nasa.gov/archive/gnss/data/) and UNAVCO (https://data.unavco.org/archive/gnss/rinex/obs/, registration required). This research was funded by the National Natural Science Foundation of China (no. 42230104, no. 42425003) and the Fundamental Research Funds for the Central Universities (no. 2042023kf0179). The numerical calculations have been done on the supercomputing system in the Supercomputing Center of Wuhan University. We thank Yuhang Yang, Jianfeng Wu, Yu Guo and Zhiyu Zhang for their helpful discussions.

References

Aa, E., Coster, A. J., Zhang, S. R., Vierinen, J., Erickson, P. J., Goncharenko, L. P., & Rideout, W. (2024a). 2-D total electron content and 3-D ionospheric electron density variations during the 14 October 2023 annular solar eclipse. *Journal of Geophysical Research: Space Physics*, 129(3), e2024JA032447. doi: 10.1029/2024JA032447

Aa, E., Huba, J., Zhang, S. R., Coster, A. J., Erickson, P. J., Goncharenko, L. P., ... & Rideout, W. (2024b). Multi-instrument and SAMI3 - TIDAS data assimilation analysis of three - dimensional ionospheric electron density variations during the April 2024 total solar eclipse. *Journal of Geophysical Research: Space Physics*, 129(9), e2024JA032955. doi: 10.1029/2024JA032955

Aa, E., Zhang, S. R., Erickson, P. J., Goncharenko, L. P., Coster, A. J., Jonah, O. F., ... & Liu, L. (2020). Coordinated ground-based and space-borne observations of ionospheric response to the annular solar eclipse on 26 December 2019. *Journal of Geophysical Research: Space Physics*, 125(11), e2020JA028296. doi: 10.1029/2020JA028296

Aa, E., Zhang, S. R., Shen, H., Liu, S., & Li, J. (2021). Local and conjugate ionospheric total electron content variation during the 21 June 2020 solar eclipse. *Advances in Space Research*, 68(8), 3435-3454. doi: 10.1016/j.asr.2021.06.015

Afraimovich, E. L., Palamartchouk, K. S., Perevalova, N. P., Chernukhov, V. V., Lukhnev, A. V., & Zalutsky, V. T. (1998). Ionospheric effects of the solar eclipse of March 9, 1997, as deduced from GPS data. *Geophysical research letters*, 25(4), 465-468. doi: 10.1029/98GL00186

Baran, L. W., Ephishov, I. I., Shagimuratov, I. I., Ivanov, V. P., & Lagovsky, A. F. (2003). The response of the ionospheric total electron content to the solar eclipse on August 11, 1999. *Advances in Space Research*, 31(4), 989-994. doi: 10.1016/S0273-1177(02)00885-2

Baron, M. J., & Hunsucker, R. D. (1973). Incoherent scatter radar observations of the auroral zone ionosphere during the total solar eclipse of July 10, 1972. *Journal of Geophysical Research*, 78(31), 7451-7460. doi: 10.1029/JA078i031p07451

Boitman, O. N., Kalikhman, A. D., & Tashchilin, A. V. (1999). The midlatitude ionosphere during the total solar eclipse of March 9, 1997. *Journal of Geophysical Research: Space Physics*, 104(A12), 28197-28206. doi: 10.1029/1999JA900228

Boitman, O. N., Kalikhman, A. D., & Tashchilin, A. V. (1999). The midlatitude ionosphere during the total solar eclipse of March 9, 1997. *Journal of Geophysical Research: Space Physics*, 104(A12), 28197-28206. doi: 10.1029/1999JA900228

Bullett, T., & Mabie, J. (2018). Vertical and oblique ionosphere sounding during the 21 August 2017 solar eclipse. *Geophysical Research Letters*, 45(8), 3690-3697. doi: 10.1002/2018GL077413

Chen, C. H., Lin, C. C., Lee, C. J., Liu, J. Y., & Saito, A. (2022). Ionospheric responses on the 21 August 2017 solar eclipse by using three-dimensional GNSS tomography. *Earth, Planets and Space*, 74(1), 173. doi: 10.1186/s40623-022-01734-y

Chen, G., Qi, H., Ning, B., Zhao, Z., Yao, M., Deng, Z., ... & Wu, C. (2013). Nighttime ionospheric enhancements induced by the occurrence of an evening solar eclipse. *Journal of Geophysical Research: Space Physics*, 118(10), 6588-6596. doi: 10.1002/jgra.50551

Chen, G., Zhao, Z., Yang, G., Zhou, C., Yao, M., Li, T., ... & Li, N. (2010). Enhancement and HF Doppler observations of sporadic-E during the solar eclipse of 22 July 2009. *Journal of Geophysical Research: Space Physics*, 115(A9). doi: 10.1029/2010JA015530

Cheng, K., Huang, Y. N., & Chen, S. W. (1992). Ionospheric effects of the solar eclipse of September 23, 1987, around the equatorial anomaly crest region. *Journal of Geophysical Research: Space Physics*, 97(A1), 103-111. doi: 10.1029/91JA02409

Cherniak, I., & Zakharenkova, I. (2018). Ionospheric total electron content response to the great American solar eclipse of 21 August 2017. *Geophysical Research Letters*, 45(3), 1199-1208. doi: 10.1002/2017GL075989

Ciraolo, L., Azpilicueta, F., Brunini, C., Meza, A., & Radicella, S. M. (2007). Calibration errors on experimental slant total electron content (TEC) determined with GPS. *Journal of Geodesy*, 81, 111-120. doi: 10.1007/s00190-006-0093-1

Coster, A. J., Goncharenko, L., Zhang, S. R., Erickson, P. J., Rideout, W., & Vierinen, J. (2017). GNSS observations of ionospheric variations during the 21 August 2017 solar eclipse. *Geophysical Research Letters*, 44(24), 12-041. doi: 10.1002/2017GL075774

Dang, T., Lei, J., Wang, W., Zhang, B., Burns, A., Le, H., ... & Wan, W. (2018). Global responses of the coupled thermosphere and ionosphere system to the August 2017 Great American Solar Eclipse. *Journal of Geophysical Research: Space Physics*, 123(8), 7040-7050. doi: 10.1029/2018JA025566

Ding, F., Wan, W., Ning, B., Liu, L., Le, H., Xu, G., ... & Yang, M. (2010). GPS TEC response to the 22 July 2009 total solar eclipse in East Asia. *Journal of Geophysical Research: Space Physics*, 115(A7). doi: 10.1029/2009JA015113

Evans, J. V. (1965). On the behavior of f_0F_2 during solar eclipses. *Journal of Geophysical Research*, 70(3), 733-738. doi: 10.1029/JZ070i003p00733

Huang, C. R., Liu, C. H., Yeh, K. C., Lin, K. H., Tsai, W. H., Yeh, H. C., & Liu, J. Y. (1999). A study of tomographically reconstructed ionospheric images during a solar eclipse. *Journal of Geophysical Research: Space Physics*, 104(A1), 79-94. doi: 10.1029/98JA02531

Huang, F., Li, Q., Shen, X., Xiong, C., Yan, R., Zhang, S. R., ... & Lei, J. (2020). Ionospheric responses at low latitudes to the annular solar eclipse on 21 June 2020. *Journal of Geophysical Research: Space Physics*, 125(10), e2020JA028483. doi: 10.1029/2020JA028483

Huba, J. D., & Drob, D. (2017). SAMI3 prediction of the impact of the 21 August 2017 total solar eclipse on the ionosphere/plasmasphere system. *Geophysical Research Letters*, 44(12), 5928-5935. doi: 10.1002/2017GL073549

Hussien, F., Ghamry, E., Fathy, A., & Mahrous, S. (2020). Swarm satellite observations of the 21 August 2017 solar eclipse. *Journal of Astronomy and Space Sciences*, 37(1), 29-34. doi: 10.5140/JASS.2020.37.1.29

Kundu, S., Chowdhury, S., Palit, S., Mondal, S. K., & Sasmal, S. (2022). Variation of ionospheric plasma density during the annular solar eclipse on December 26, 2019. *Astrophysics and Space Science*, 367(5), 44. doi: 10.1007/s10509-022-04069-y

Le, H., Liu, L., Ren, Z., Chen, Y., & Zhang, H. (2020). Effects of the 21 June 2020 solar eclipse on conjugate hemispheres: A modeling study. *Journal of Geophysical Research: Space Physics*, 125(11), e2020JA028344. doi: 10.1029/2020JA028344

Lei, J., Dang, T., Wang, W., Burns, A., Zhang, B., & Le, H. (2018). Long-lasting response of the global thermosphere and ionosphere to the 21 August 2017 solar eclipse. *Journal of Geophysical Research: Space Physics*, 123(5), 4309-4316. doi: 10.1029/2018JA025460

Lin, C. Y., Deng, Y., & Ridley, A. (2018). Atmospheric gravity waves in the ionosphere and thermosphere during the 2017 solar eclipse. *Geophysical Research Letters*, 45(11), 5246-5252. doi: 10.1029/2018GL077388

Mei, D., Ren, X., Le, X., Liu, H., & Zhang, X. (2023). Ionospheric tomography: A compressed sensing technique based on dictionary learning. *IEEE Transactions on Geoscience and Remote Sensing*, 61, 1-10. doi: 10.1109/TGRS.2023.3252041

Mishin, E., Sutton, E., Milikh, G., Galkin, I., Roth, C., & Förster, M. (2012). F2-region atmospheric gravity waves due to high-power HF heating and subauroral polarization streams. *Geophysical research letters*, 39(11). doi: 10.1029/2012GL052004

Moses, M. L., Kordella, L. J., Earle, G. D., Drob, D., Huba, J. D., Ruohoniemi, J. M., ... & Sivakumar, V. (2021). Observations and modeling studies of solar eclipse effects on oblique high frequency radio propagation. *Space Weather*, 19(3), e2020SW002560. doi: 10.1029/2020SW002560

Müller-Wodarg, I. C. F., Aylward, A. D., & Lockwood, M. (1998). Effects of a mid‐latitude solar eclipse on the thermosphere and ionosphere-A modelling study. *Geophysical Research Letters*, 25(20), 3787-3790. doi: 10.1029/1998GL900045

Panasenko, S. V., Otsuka, Y., van de Kamp, M., Chernogor, L. F., Shinbori, A., Tsugawa, T., & Nishioka, M. (2019). Observation and characterization of traveling ionospheric disturbances induced by solar eclipse of 20 March 2015 using incoherent scatter radars and GPS networks. *Journal of Atmospheric and Solar-Terrestrial Physics*, 191, 105051. doi: 10.1016/j.jastp.2019.05.015

Perry, G. W., Watson, C., Howarth, A. D., Themens, D. R., Foss, V., Langley, R. B., & Yau, A. W. (2019). Topside ionospheric disturbances detected using radio occultation measurements during the August 2017 solar eclipse. *Geophysical Research Letters*, 46(13), 7069-7078. doi: 10.1029/2019GL083195

Pradipta, R., Yizengaw, E., & Doherty, P. (2018). Ionospheric density irregularities, turbulence, and wave disturbances during the total solar eclipse over North America on 21 August 2017. *Geophysical Research Letters*, 45(16), 7909-7917. doi: 10.1029/2018GL079383

Reinisch, B. W., Dandenault, P. B., Galkin, I. A., Hamel, R., & Richards, P. G. (2018). Investigation of the electron density variation during the 21 August 2017 solar eclipse. *Geophysical Research Letters*, 45(3), 1253-1261. doi: 10.1002/2017GL076572

Ren, X., Le, X., Mei, D., Liu, H., & Zhang, X. (2024). IROTI: a new index to detect and identify traveling ionospheric disturbances and equatorial plasma bubbles. *GPS Solutions*, 28(1), 7. doi: 10.1007/s10291-023-01545-y

Tsai, H. F., & Liu, J. Y. (1999). Ionospheric total electron content response to solar eclipses. *Journal of Geophysical Research: Space Physics*, 104(A6), 12657-12668. doi: 10.1029/1999JA900001

Tsai, H. F., & Liu, J. Y. (1999). Ionospheric total electron content response to solar eclipses. *Journal of Geophysical Research: Space Physics*, 104(A6), 12657-12668. doi: 10.1029/1999JA900001

Vierinen, J., Coster, A. J., Rideout, W. C., Erickson, P. J., & Norberg, J. (2016). Statistical framework for estimating GNSS bias. *Atmospheric Measurement Techniques*, 9(3), 1303-1312. doi: 10.5194/amt-9-1303-2016

Vyas, B. M., & Sunda, S. (2012). The solar eclipse and its associated ionospheric TEC variations over Indian stations on January 15, 2010. *Advances in space research*, 49(3), 546-555. doi: 10.1016/j.asr.2011.11.009

Wu, C., Ridley, A. J., Goncharenko, L., & Chen, G. (2018). GITM-data comparisons of the depletion and enhancement during the 2017 solar eclipse. *Geophysical Research Letters*, 45(8), 3319-3327. doi: 10.1002/2018GL077409

Zhang, R., Le, H., Li, W., Ma, H., Yang, Y., Huang, H., ... & Liu, L. (2020). Multiple technique observations of the ionospheric responses to the 21 June 2020 solar eclipse. *Journal of Geophysical Research: Space Physics*, 125(12), e2020JA028450. doi: 10.1029/2020JA028450

Zhang, S. R., Erickson, P. J., Goncharenko, L. P., Coster, A. J., Rideout, W., & Vierinen, J. (2017). Ionospheric bow waves and perturbations induced by the 21 August 2017 solar eclipse. *Geophysical Research Letters*, 44(24), 12-067. doi: 10.1002/2017GL076054

Zhang, S. R., Erickson, P. J., Vierinen, J., Aa, E., Rideout, W., Coster, A. J., & Goncharenko, L. P. (2021). Conjugate ionospheric perturbation during the 2017 solar eclipse. *Journal of Geophysical Research: Space Physics*, 126(2), e2020JA028531. doi: 10.1029/2020JA028531

Declaration of Interest Statement

The authors declare that they have no known competing financial interests or personal relationships that could have appeared to influence the work reported in this paper.